Observations of Transient Linear Organization and Nonlinear Scale Interactions in Lake-Effect Clouds. Part I: Transient Linear Organization

NATASHA L. MILES AND JOHANNES VERLINDE

Department of Meteorology, The Pennsylvania State University, University Park, Pennsylavania

(Manuscript received 2 September 2003, in final form 10 August 2004)

ABSTRACT

The cold-air outbreak of 13–14 January 1998 during the Lake-Induced Convection Experiment was characterized by large positive buoyancy flux and moderate wind shear. Although theory predicts only cellular organization in these conditions, transient linear organization was observed. Time series of vertical velocity obtained with the Pennsylvania State University 94-GHz vertically pointing cloud radar, which is sensitive to cloud droplets and ice crystals, were used to document the changes in organization that occurred during this wintertime lake-effect event. The cloud radar was deployed on the downwind shore of southern Lake Michigan and measured high-temporal-resolution vertical velocity data at several in-cloud heights. The duration of the event was 18 h, encompassing three cycles of linear organization switching to cellular organization.

In Part I of this two-part series the authors document the transient nature of the linearly organized convection and evaluate the role of atmospheric conditions in the mode switching between linear and cellular organization. Within the limits of the available measurements, no correlation was found with mean or low-level shear, surface fluxes, or stability parameters. The mode switching in this case does not appear to be controlled by the atmospheric indicators typically associated with linearly organized convection, suggesting that other factors must have played an important role.

1. Introduction

Linear organization in the form of horizontal roll vortices is a common feature in the atmospheric boundary layer under windy conditions and has been the subject of numerous studies (e.g., see reviews by Etling and Brown 1993; Atkinson and Zhang 1996; Young et al. 2002). While much progress in understanding the dynamics of these systems has been made, much is still unclear. For instance, while it is understood that convective mixed-layer roll vortices tend to develop in environments characterized by weak thermal instability and high wind shear (e.g., Deardorff 1972; LeMone 1973; Grossman 1982; Sykes and Henn 1989; Weckwerth et al. 1997; Khanna and Brasseur 1998; Glendening 2000), other studies (e.g., Kelly 1984; Kristovich 1993; Christian and Wakimoto 1989; Ferrare et al. 1991) have indicated that rolls can occur in very unstable conditions.

In this set of two papers, we examine convective organization in a lake-effect event over Lake Michigan that, instead of having a single dominant organizational mode, switched between marginally linear organization and more random cellular organization. Environmental conditions during this lake-effect event were atypical for linear organization—the surface buoyancy flux was very large and the shear was only moderate. In this paper, we document the transient nature of the case and evaluate possible causes for these changes in organization, and in Part II (Miles and Verlinde 2005, hereafter referred to as Part II) we investigate interactions between scales at different stages of organization.

Although such observations are not common, cases of "mode switching" between linear and nonlinear organization have been documented. For example, Braham (1986) reported radar observations of linear patterns persisting for 2 h until changing to cellular patterns. The linear patterns were reestablished after 3 h, but the orientation had shifted by 45°. Weckwerth et al. (1999) documented several cases of well-organized roll organization evolving into more cellular organization. Kristovich et al. (1999) observed transitions from predominantly cellular convection, to linearly organized convection, and back to a mixture of nonrolls and rolls in their study of boundary layer rolls over Lake Michigan.

This study of convective organization mode switching is unique in its long duration of continuous high-

Corresponding author address: Dr. Natasha L. Miles, Dept. of Meteorology, College of Earth and Mineral Sciences, The Pennsylvania State University, 503 Walker Building, University Park, PA 16802.
E-mail: nmiles@met.psu.edu

resolution vertical velocity data. Eighteen hours of 94-GHz Doppler cloud radar vertical velocity data, collected every 7.5 s at around 10 in-cloud heights, were measured on the downwind shore of southern Lake Michigan during the Lake-Induced Convection Experiment (Lake-ICE).

2. The dataset

The data used in this study were measured during Lake-ICE, which was conducted in the vicinity of Lake Michigan during December 1997–January 1998 (Kristovich et al. 2000). The primary data for this study are air vertical velocities retrieved from the Pennsylvania State University (PSU) cloud radar data. The analysis period begins when the cloud radar became operational at 1217 UTC on 13 January and extends nearly 18 h until 0556 UTC on 14 January.

As part of Lake-ICE, the PSU 94-GHz (3-mm wavelength) Doppler cloud radar was deployed to the Great Lakes Environmental Research Laboratory Lake Michigan Field Station in Muskegon, Michigan, about 10 m from the water edge. The radar system, described by Clothiaux et al. (1995), is bistatic (i.e., it has separate transmitting and receiving antennae) with a beamwidth of 0.24° for each antenna. The vertically pointing radar has a footprint of approximately 3 m for a typical in-cloud height of 750 m. The along-wind dimension of the radar resolution volume is larger, about 50 m, since the mean wind advects the cloudy air through the radar resolution volume for the duration of the sampling period and processing time (7.5 s total). The vertical resolution of the radar is 30 m.

Operating at a higher frequency than a typical weather radar, the cloud radar is sensitive to hydrometeors ranging in size from the small cloud droplets and ice crystals in continental stratocumulus clouds to the larger drops and crystals in precipitation. The cloud radar data were processed to obtain Doppler spectra (reflectivity as a function of vertical velocity) and filtered through a cloud mask (Clothiaux et al. 1995). Each Doppler spectrum is the quiet-air fall velocity spectrum of the cloud particles (the spectrum that would be measured if the air were perfectly still) broadened by turbulent motions within the radar resolution volume and shifted by the mean vertical velocity in the radar resolution volume. We use the deconvolution technique developed by Babb et al. (2000) to remove the turbulent broadening effects. To obtain the volume mean wind, we assume the smallest hydrometeors detected by the radar are tracers of the wind, having negligible fall velocity. The mean air vertical velocity in the radar resolution volume is then simply the shift from zero of the (slow falling) edge of the spectrum on the velocity axis. The uncertainty of the retrieved air vertical velocity is 0.1 m s^{-1} (Figs. 9 and 12 in Babb et al. 2000) and the uncertainty of the vertical velocity variance is 0.01 m^2 s^{-2} (Fig. 15 in Babb et al. 2000).

There are two aspects of the cloud radar itself and the data-collection scheme that are not ideal. Because the radar is bistatic, the volume that is "illuminated" by the transmitting antenna does not exactly coincide with the volume from which the receiving antenna can receive a signal. The measured radar reflectivity is thus lower than the actual reflectivity. Fortunately, the magnitude of the reflectivity has little effect on the deconvolution technique; we only need to know the measured vertical velocity of the smallest droplets.

The second problematic aspect of the cloud radar is that the data were recorded only every 7.5 s. Although this resolution is very high compared to some studies, Giangrande et al. (2001) reported that changes in the vertical wind speed during the sampling period can broaden the measured Doppler spectra. The deconvolution technique removes the effects of turbulent broadening and may also remove some of the broadening effects incurred during the sampling period. It is likely, however, that some broadening effects remain. If there is broadening not removed by the analysis, the retrieved mean vertical velocity within the volume will be too high. In the present case, the mean vertical velocity, averaged throughout the analysis period and from cloud base to cloud top, is about 0.5 m s^{-1}. The cause is a combination of frictional convergence at the shore (e.g., Holroyd 1971), positive buoyancy from the lake, and the aforementioned broadening effects induced by changes in the vertical velocity during the sampling period.

A drawback to the use of a vertically pointing cloud radar is the inability to definitively distinguish between two- and three-dimensional convection. To circumvent this problem, Weather Surveillance Radar-1988 Doppler (WSR-88D) radar reflectivity data were used to establish the types of convective organization. The closest available WSR-88D was in Grand Rapids, Michigan, approximately 60 km from the Muskegon cloud radar site. At this distance, only data from the lowest elevation angle, 0.5°, were in-cloud; thus only one nearly horizontal slice of reflectivity data was usable. The data were interpolated onto a 16 km × 16 km Cartesian grid with 500-m horizontal resolution using the National Center for Atmospheric Research (NCAR) Reorder software package (Oye and Case 1994). A Cressman (1959) filter with a radius of influence of 1.0 km was used in the interpolation.

Two NCAR Integrated Sounding Systems (ISS) were deployed during Lake-ICE, one in Montague, Michigan (on the downwind shore) and the other in Sheboygan, Wisconsin (on the upwind shore; Fig. 1). At these sites, 915-MHz Doppler clear-air wind-profiling radars recorded profiles of horizontal and vertical winds at 30-min intervals and 56-m vertical resolution. The profiler data were available at heights between 95 and 375 m for the upwind site and between 53 and 837 m for the downwind site. Surface meteorological stations collected 1-min measurements of pressure, temperature,

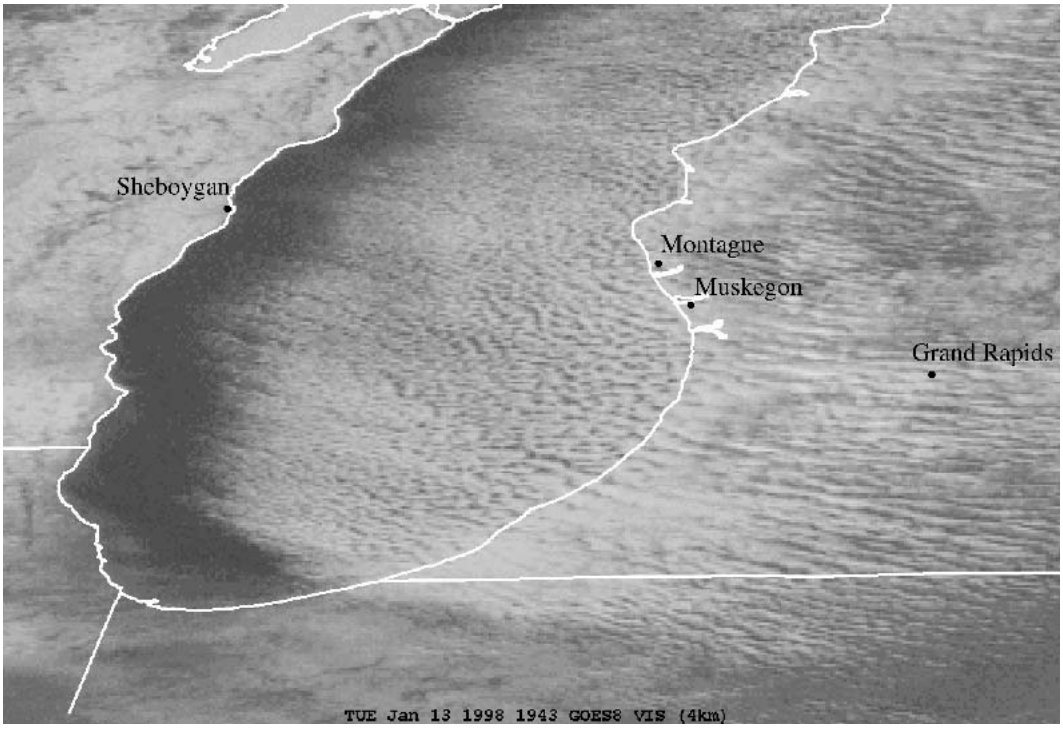

FIG. 1. *GOES-8* satellite image showing the convective organization over the southern Lake Michigan vicinity at 1943 UTC on 13 Jan 1998. The location of the cloud radar at Muskegon, MI, is shown, as well as the ISS sites at Montague, MI, and Sheboygan, WI, and the WSR-88D site in Grand Rapids, MI.

relative humidity, horizontal wind speed, and wind direction. Temperature and relative humidity were measured at a height of 2 m AGL, pressure at 1.75 m AGL, and the wind data at 10 m AGL. Cross-Chain Loran Atmospheric Sounding System (CLASS) radiosondes were released from the Montague and Sheboygan ISS sites, as well as from the Muskegon cloud radar site.

The Montague ISS site was located 21 km north-northwest of the cloud radar site. Its wind data are, unfortunately, substantially influenced by topography. Whereas the Muskegon cloud radar site was on the lake shore, the Montague ISS site was 1–2 km inland, downwind of sand dunes, plaguing primarily the low-level shear values, and to a lesser extent the boundary layer mean shear values.

A Vaisala laser ceilometer at the Muskegon site recorded cloud-base heights with vertical resolution of 15 m every 30 sec. Between 15% and 20% of the measurements were contaminated by hydrometeors falling below cloud base; thus points more than one standard deviation from the mean were excluded.

The boundary layer depth (z_i) was determined in two ways: 1) from the soundings using the height of the base of the overlying stable layer, and 2) from the cloud radar data using the cloud-top height (e.g., Walter 1980). The cloud-top height was determined using a method similar to that described in a lidar study by Kiemle et al. (1998). A histogram of the number of samples (throughout the analysis period) within a reflectivity bin was plotted as a function of reflectivity and height, revealing two groups. The majority of the samples in the higher-altitude group were between −54 dBZe and −44 dBZe, representing the noise level measured above cloud top. Thus cloud top was defined as the highest height with reflectivity greater than −44 dBZe. The units dBZe refer to the equivalent reflectivity factor, which is the reflectivity factor of a population of liquid and spherical particles producing a signal of the same power as the mixed phase particles actually measured. Except during periods with broken clouds, the smoothed cloud-top height agreed with the radiosonde inversion base height to within the radar resolution. Other authors (e.g., Weckwerth et al. 1997) have estimated the boundary layer depth as the height at which there was a change in the slope of the reflectivity plotted as a function of height. The error associated with each of the methods is similar. The high-resolution z_i determined from the radar measurements was used for the Montague ISS site. For the Sheboygan site, the average inversion height as determined from the soundings was used.

Between 1400 and 1700 UTC on 13 January 1998, the NCAR Electra aircraft flew roughly east–west horizontal flight legs across the northern part of Lake Michigan. Young et al. (2000) discuss the in situ aircraft results from Lake-ICE and Kristovich et al. (2003)

present Electra Doppler Radar (ELDORA) dual-Doppler results, but aircraft restrictions on that day did not allow flight patterns near the Muskegon cloud radar site, making comparisons difficult to interpret (Miles 2002).

3. WSR-88D radar-observed transient linear organization

The lake-effect event on 13–14 January 1998 was associated with large sensible and latent heat fluxes and moderate wind speeds. At the downwind shore, the total (sensible plus latent) heat flux averaged about 350 W m^{-2} during the event (calculated using bulk transfer formulas; see section 5b), and the surface wind speed averaged about 6 m s^{-1} from the northwest. The event was relatively uncontaminated by large-scale ascent and frontal clouds, as evidenced by the clear skies on the upwind shore in the satellite image (Fig. 1).

Widespread lake-effect clouds were generated over Lake Michigan on 13 January following the passage of a shallow, but vigorous cold front around 1800 UTC on 12 January. The National Oceanic and Atmospheric Administration (NOAA) surface analysis for 1200 UTC on 13 January is available in Kristovich et al. (2003; their Fig. 4). Lake surface temperatures, from satellite data observed between 24 December 1997 and 25 January 1998, varied from +2°C on the upwind shore to +5°C on the downwind shore. The lake surface temperature averaged along a line between Muskegon and the shore upwind of Muskegon was +4°C. Temperature differences between the lake and 850 mb were between 18° and 22°C, well above the minimum temperature difference of 13°C required for lake-effect snow (e.g., Braham 1983; Niziol 1987; Burrows 1991). In lake-effect conditions, the boundary layer depth increases rapidly across the lake because of the large amount of buoyancy introduced (Agee and Gilbert 1989; Chang and Braham 1991; Kristovich et al. 1999; Young et al. 2000). In this case, potential temperature profiles (Kristovich et al. 2003, their Fig. 5a) suggest a convective boundary layer of depth around 340 m near the upwind shore for the Sheboygan ISS site. The average radar-derived cloud-top height on the downwind shore in Muskegon was 890 m, and the average ceilometer-derived cloud-base height in Muskegon was 630 m (Fig. 2). The evolution of the basic surface meteorological parameters are shown in Fig. 3 for the ISS sites upwind of the lake in Sheboygan (Figs. 3a–d) and downwind of the lake in Montague (Figs. 3e–h). The time of each upwind parcel to arrive at the downwind shore is estimated using the time-varying upwind boundary layer mean wind speed.

The *Geostationary Operational Environmental Satellite-8* (*GOES-8*) visible satellite image at 1943 UTC shows well-defined rolls over land downstream of Lake Michigan (Fig. 1). The more cellular, but still linearly aligned, appearance of the rolls over the lake is consistent with the larger heat and moisture flux over the lake compared to the land. Frictional convergence at the downwind shoreline results in air lifting along the shore and a comparatively homogeneous appearance near the shoreline. In the vicinity of the location of the cloud radar in Muskegon, faint cloud streets are apparent. The wavelength of the rolls visible in Fig. 1 is 5–10 km.

Examples of WSR-88D reflectivity fields at 1301, 1601, and 1751 UTC on 13 January 1998 are shown in Figs. 4a, 4c, and 4e, respectively. Muskegon is near the western limit of the range for the Grand Rapids WSR-88D; thus our WSR-88D analysis domain is situated such that the position of the cloud radar was at the center of the western edge, at $x = -16$ km and $y = 0$ km (indicated in Figs. 4a, 4c, and 4e by white squares). This shift necessitates a time correction between the WSR-88D and Muskegon data. The times associated with the WSR-88D images (those indicated above and hereafter) are adjusted by the approximate time required for a parcel to advect from a point that is upwind of the center of the WSR-88D image to the center of the image. Using the mean in-cloud wind speed and wind direction during the analysis period, the calculated time correction is 62 min. The times, however, must be viewed as estimates because of the changing wind speed throughout the analysis period.

These images depict a transition from relatively organized linear convection to more cellular, disorga-

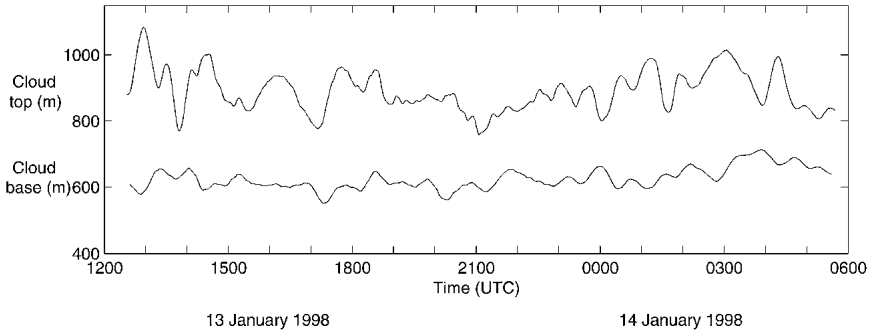

FIG. 2. Cloud-radar-derived cloud-top height and ceilometer-derived cloud base on the downwind shore in Muskegon. A running-average window length of 20 min was used.

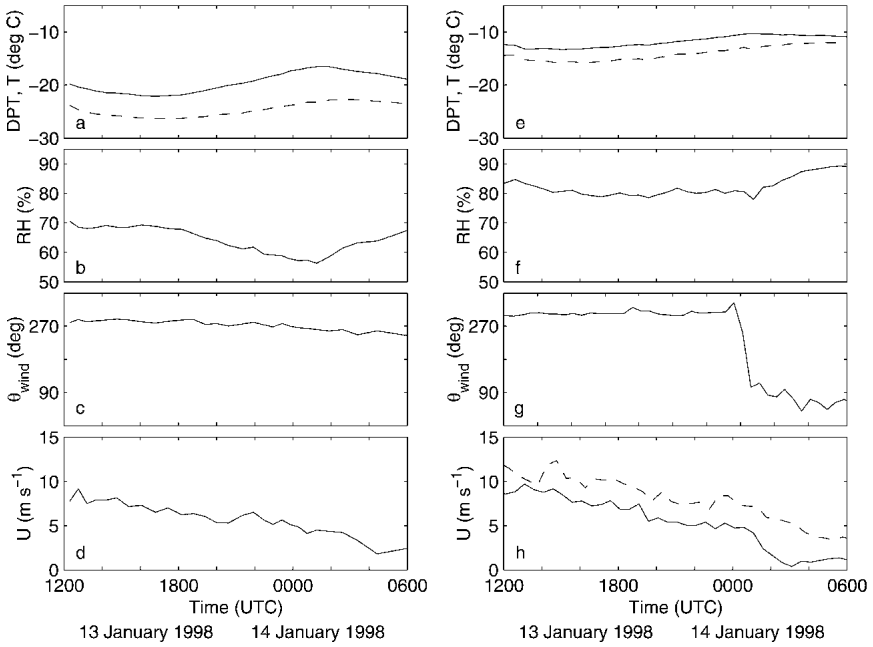

FIG. 3. Sheboygan (upwind) ISS surface data: (a) surface air temperature (solid line) and dewpoint temperature (dashed line), (b) relative humidity, (c) surface wind direction, and (d) surface horizontal wind speed. (e)–(h) Corresponding surface data for Montague (downwind). In (h), the cloud layer mean wind speed is represented by the dashed line. The times indicated in (a)–(d) are the estimated times that the parcels from the upwind shore reached the downwind shore.

nized convection, and back to marginally linear organization within a 5-h time frame. The rolls are more accurately described as radar reflectivity cells aligned in rows, as has been observed in many studies (e.g., Kuettner 1959, 1971; LeMone 1973; Braham and Kristovich 1996). The rolls are finite in length and frequently merge and change direction (e.g., Kristovich 1993; Brooks and Rogers 1997). The predominant size of the reflectivity cells is 3–5 km, only slightly smaller than the wavelength of the rolls (shown below to be 6.3 ± 0.8 km).

To quantify the linearity of the WSR-88D reflectivity images, we consider their two-dimensional autocorrelation as has been done by numerous authors (e.g., Ferrare et al. 1991; Weckwerth et al. 1997; Lohou et al. 1998; Kristovich et al. 1999). Examples of the two-dimensional autocorrelation fields are shown in Figs. 4b, 4d, and 4f. The ratio of the length of the major axis of a central contour to that of the minor axis [horizontal aspect ratio (HAR); Weckwerth et al. 1997] gives a measure of the linearity, with values near one expected for cellular structure and higher values expected for rolls. The calculated HAR values for the 0.4 autocorrelation contours are shown in Fig. 5a. For their analysis of dual-Doppler radar reflectivity images, both Weckwerth et al. (1997) and Kristovich et al. (1999) use the 0.2 contour rather than the 0.4 contour used in this case. Compared to the Weckwerth et al. (1997) case, the reflectivity observed in this study is more homogeneous. Thus the autocorrelation does not decrease as much between the rolls, necessitating the use of the higher contour to more accurately describe the differences in organization. For example, for the autocorrelation field shown in Fig. 4f, the 0.2 contour is nearly as large as the entire domain. As noted by Ferrare et al. (1991), for well-organized cases such as that shown in Fig. 4b, the HAR calculated using the 0.2 contour is comparable to that calculated using the 0.4 contour; thus the choice of contour is somewhat arbitrary.

None of the values calculated in this study meet the criteria for rolls (HAR $\geq$ 6) set by Weckwerth et al. (1997) for their clear-air dual-Doppler analysis. Nevertheless, there are clear trends in the HAR time series (Fig. 5a) that are consistent with visual analysis of the images. From the beginning of the analysis period until about 1500 UTC, the values for HAR vary between 2 and 4. Between 1500 and 1720 UTC, the HAR is much lower, about 1.4, before rising again to about 4 during the period from 1720 to 1930 UTC. After 1930 UTC, the HAR is again low, clustered around 1.4, with a few scattered points with HAR up to 3. The HAR results and their comparison with the linearity as determined through the cloud radar data are discussed in section 4.

At 0140 UTC, the mean of the WSR-88D reflectivity drops considerably. This drop in reflectivity coincides with the development of a weak land breeze, associated

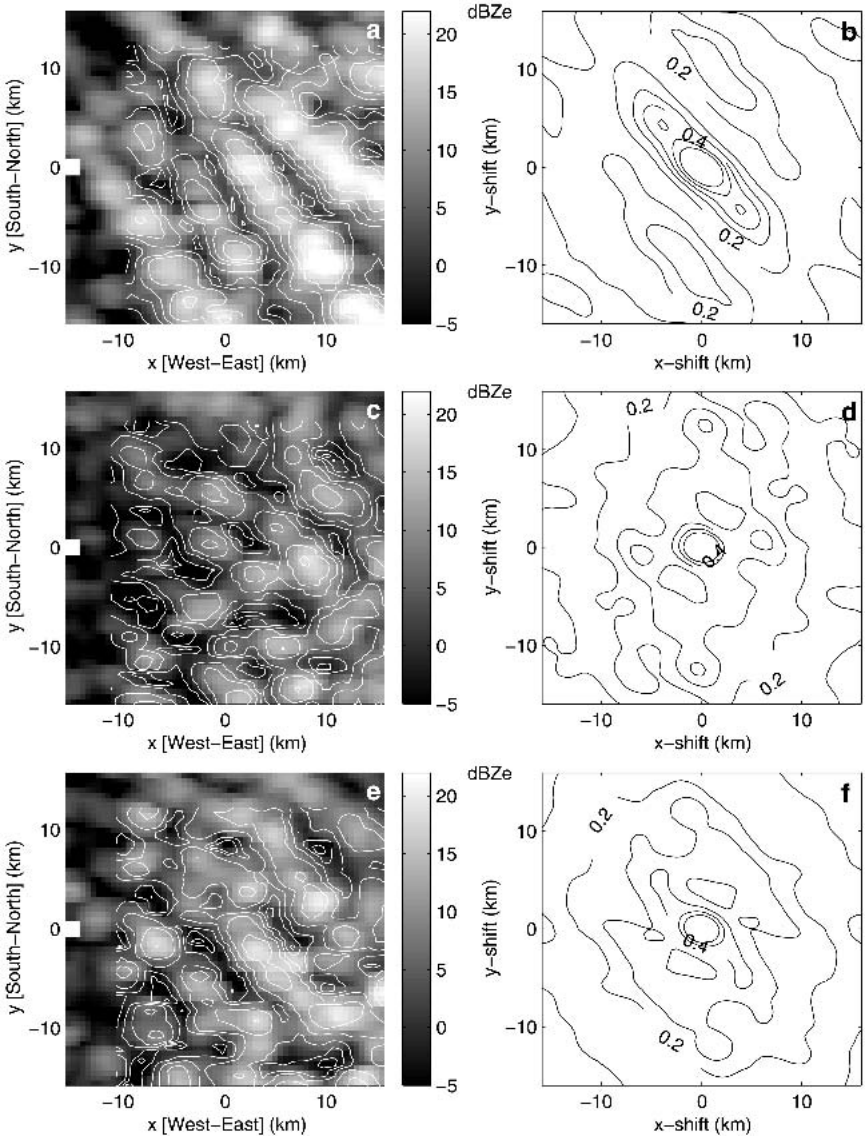

FIG. 4. (left) Examples of WSR-88D reflectivity fields at (a) 1301, (c) 1601, and (e) 1751 UTC on 13 Jan 1998. The position of the PSU cloud radar is indicated by white squares at $x = -16$ km and $y = 0$. White contours represent the reflectivity field from the prior scan, shifted by the echo motion determined using cross-correlation analysis. (right) The corresponding autocorrelation fields at (b) 1301, (d) 1601, and (f) 1751 UTC. Contours of multiples of 0.1 are shown, starting with 0.6 in the center and decreasing to 0.1. All times are adjusted times.

with decreases in wind speed, fluxes, and thus precipitation development at that time. The values of HAR after 0140 UTC have thus been excluded from Fig. 5a.

In general, the HAR values calculated here are low compared to other studies, suggesting that the linear organization is marginal. The HAR analysis indicates that the organization of the system switched between roughly linear and predominantly cellular, never quite reaching a well-organized state.

Roll orientation and wavelength are determined from the autocorrelation fields for those images depicting linear structure. The roll orientation angle is 321° ± 11° throughout the analysis period, excluding times during which the organization is primarily cellular. The roll orientation angle is thus about 16° from the average wind direction (305°), which is within the range of typically observed values [between −20° and 30° (Etling and Brown 1993)]. The average roll wavelength, also determined from the autocorrelation fields, is 6.3 ± 0.8 km during the analysis period. The average aspect ratio (AR), defined as the roll wavelength divided by the boundary layer depth, is 7.1 ± 0.9. Other authors have

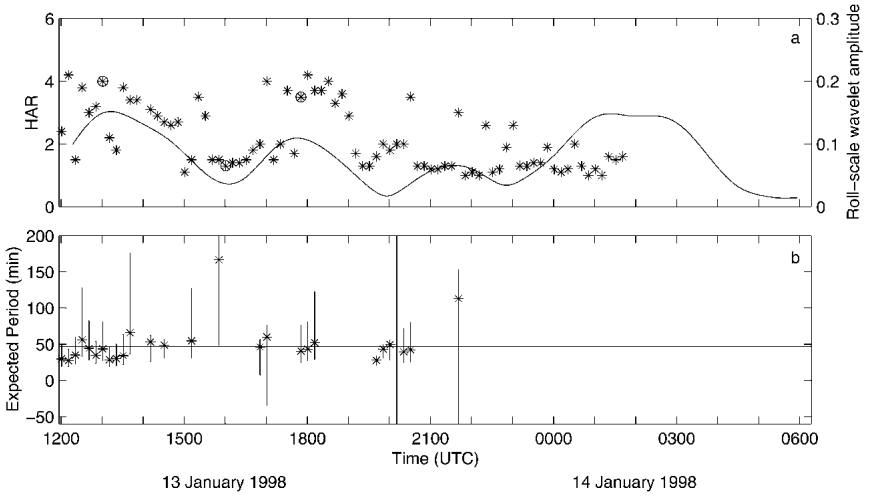

FIG. 5. (a) On the left-hand axis, the stars represent the HAR as a function of time. Circled stars indicate the values of HAR at the times shown in Fig. 4 (4.0, 1.3, and 3.5, respectively). On the right-hand axis, the solid curve is the wavelet amplitude at roll scales as determined by wavelet analysis of the cloud radar vertical velocity. (b) The period at which rolls are expected to be observed by a vertically pointing instrument, based on analysis of WSR-88D reflectivity data. Error bars indicate the cumulative error resulting from error in roll orientation and wavelength and error from the resolution of the WSR-88D reflectivity images (causing error in the echo motion). The solid line at 46.8 min is the period of the rolls as determined by wavelet analysis of cloud-radar-derived vertical velocity.

found similarly high aspect ratios over Lake Michigan [e.g., LeMone 1973 (AR: 3.3–6.5); Kelly 1984 (AR: 1.0–9.1); Kristovich 1993 (AR: 2.0–6.7); Kristovich et al. 1999 (AR: 5–6)]. The range of aspect ratios in cold-air outbreaks over lakes given in the review by Young et al. (2002) is 2.2–7.5; the average value for the present case is on the high side of this range.

Following the procedures described by Ferrare et al. (1991), two-dimensional cross correlations between successive images were calculated to estimate the average echo motion. Maximization of the cross correlation yields the average speed and direction at which reflectivity fields advanced during the 10-min intervals between scans. Throughout the majority of the analysis period, the echo speed is within 1–2 m s^{-1} of the cloud layer wind speed. On the WSR-88D reflectivity images in Figs. 4a, 4c, and 4e are superimposed contours of the reflectivity field from the prior scan, shifted by the echo motion determined by the cross-correlation analysis. For example, the echo speed for the image in Fig. 4a is 11.3 m s^{-1} and the direction is 306°.

In the relatively unlikely case that the axis of the rolls is parallel to the direction of the mean wind, the axis of the rolls would not drift over the cloud radar. The rolls in this case are, however, not aligned perfectly with the direction of the mean wind, allowing the roll updrafts and roll downdrafts to be detected by a vertically pointing cloud radar. Using the calculated echo motion, roll orientation, and roll wavelength, the period expected from the measurements of a vertically pointing instrument can be determined. The roll wavelength divided by the echo speed in the direction perpendicular to the rolls yields the expected period, shown in Fig. 5b. The expected period (excluding two points with values greater than the mean plus eight standard deviations, which are not shown in the figure) is 51 ± 30 min.

4. Cloud-radar-observed transient linear organization

We now describe the transient linear organization based on the cloud radar data. From the perspective of a stationary observer (the cloud radar), the vertical velocity overhead is a superpositioning of contributions from turbulent, cloud, and mesoscale motions. With different scales and/or advection speeds, contributions from each scale will separate in the frequency domain, suggesting the use of Fourier analysis. When the mesoscale organization is intermittent, as in the observed case, the observed time series of vertical velocity will be nonstationary, and Fourier analysis fails. In an effort to extract both frequency and time information, Gabor (1946) introduced windowed Fourier analysis, which eventually led to the development of wavelet analysis. Wavelet analysis has been increasingly used in meteorology to extract both frequency and time information from nonstationary time series and is used in this study to document the existence of the different scales and their temporal evolution.

Although the measured cloud radar data include ver-

tical profiles from near cloud base to near cloud top, we first focus on the wavelet analysis of the time series of vertical velocity at one midcloud height (720 m; ~0.81 z_i). There is no particular reason to choose this height beyond its being midcloud. A Morlet wavelet, which is a sine wave modulated by a Gaussian envelope, was chosen for the analysis. The method used is described in Torrence and Compo (1998). The wavelet vertical velocity spectrum, normalized by the square of the convective velocity scale w_*, is shown in Fig. 6a. The Nyquist frequency for the data series is $1/2\delta t = 0.067$ s^{-1}, corresponding to a minimum period of 0.25 min. We use 10 octaves with four suboctaves per octave. Edge effects due to zero padding cause the points under the cone of influence to be less reliable. The wavelet transform performed with different scale resolutions and different wavelets yields similar qualitative results. The wavelet spectrum in Fig. 6a is not in area-preserving form since we focus on the time variation of each of the scales, rather than the relative contribution to the total variance by each of the scales.

The statistical significance of the wavelet spectrum was calculated through comparison to a background spectrum of red noise and by using a chi-squared test (Torrence and Compo 1998). A red-noise (increasing power with decreasing frequency) background spectrum was chosen over a white-noise (constant power with changing frequency) background spectrum since, for vertical velocity spectra with frequency ranging from the energy-containing range to the inertial subrange, power increases with decreasing frequency. For a random time series, 1% of the points will be above the 99% significance levels just by chance.

The general shapes of the peaks in power are a consequence of the flexible window size and of the fundamental limits on the minimum uncertainty to which we can know the frequency (or period) and time simultaneously (Chui 1992; Lau and Weng 1995). In the short-period region, high precision in time localization (due to small window size) is achieved at the expense of reduced frequency resolution. The opposite is true for the long-period region. The consequence for the top third of the plot is peaks that appear stretched in period, while in the bottom third they appear stretched in time. Several dominant scales are found in the wavelet vertical velocity spectrum (Fig. 6) (where the periods indicated are based on the time-averaged peaks discussed later).

(i) Turbulence scale (<8.3 min): The turbulence scale, as defined for the purposes of this study, includes scales the size of individual thermals down to the smallest time scales detectable in the dataset, namely, 0.25 min. Using the time-averaged in-cloud horizontal velocity of 7.5 m s^{-1} as an estimate and Taylor's frozen turbulence hypothesis, the approximate sizes included in the turbulence scale are 100 m–3.7 km. The 1335-m (3.0 min) scale corresponding to the typical 1.5 aspect ratio found in convective turbulence spectra (Kaimal et al. 1976) is within this range. Our "turbulence scale" contains part of the energy-containing range and part of the inertial subrange.

(ii) Cell scale (8.3–16.5 min): We use the term "cells"

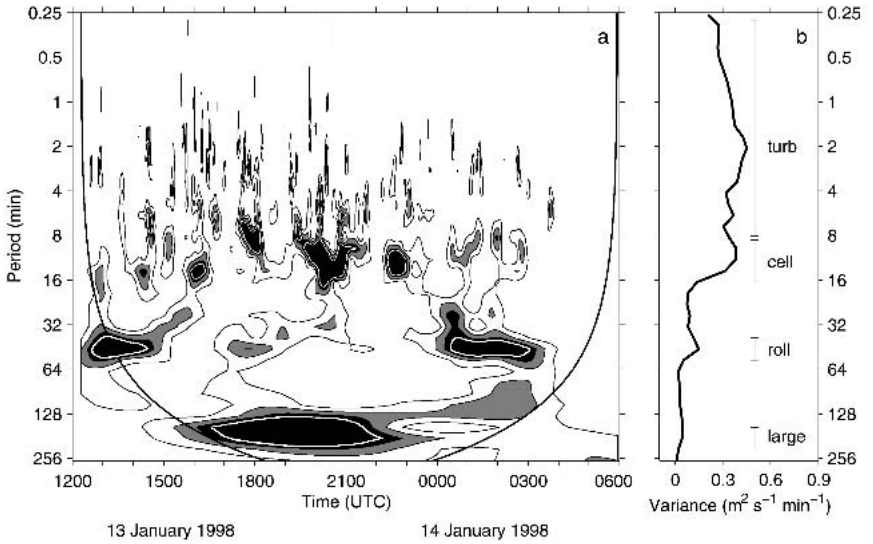

FIG. 6. (a) Wavelet vertical velocity spectrum, normalized by w_*^2, for a time series of vertical velocities at a height of 720 m (~0.81 z_i). Contours of the normalized spectrum are plotted at 2, 4, and 6. Edge effects due to zero padding cause the points under the cone of influence, shown as a solid curve, to be less reliable. Statistically significant peaks at the 99% significance level for a red-noise process are shown as white contours for periods greater than 4 min. (b) The corresponding global wavelet vertical velocity spectrum, in area-preserving form to indicate the relative contribution of each scale to the total variance.

to describe the patches of convection visible in Fig. 4. The cells in our study differ from mesoscale cells that occur over oceans and are typically 10–40 km in diameter (e.g., Atkinson and Zhang 1996) and from cores which are 100-m-scale convective elements (e.g., Braham and Kristovich 1996). Using the average in-cloud wind speed of 7.5 m s^{-1}, the sizes included in the cell-scale period range are 3.7–7.4 km, roughly in agreement with the range of reflectivity cell sizes observed in the WSR-88D images (Fig. 4). The strongest amplitude peak in the cell period range occurs at about 2035 UTC. There are nine additional local peaks, each of shorter duration. While the peaks in this range are not centered at exactly the same period, the majority have centers between 10 and 14 min. The four statistically significant (at the 99% confidence level) peaks occur at times during which the power in the roll scale is low, suggesting an inverse relationship between the cell-scale and the roll-scale activity, and possible upscale energy transfer.

(iii) Roll scale (39.3–55.6 min): The roll-scale signal exhibits amplitude modulation, with three time periods of larger amplitudes, persisting with powers above $2w_*^2$ during the times 1217–1515, 1635–1905, and 2327–0357 UTC. The average length of the three peaks is 200 min (over four oscillations). There is a hint of another peak between the second and third peaks. The first and third peaks are statistically significant at the 99% confidence level compared to a red-noise background spectrum, while the second peak is statistically significant at the 95% confidence level. As the first and second peaks diminish in amplitude, there is evidence of shifting toward higher frequencies. Although Renfrew and Moore (1999) observed rolls and cloud streets with different wavelengths, the wavelengths in this case agree fairly well; the peaks are within the range of periods expected according to the WSR-88D analysis (Fig. 5b). The average roll wavelength determined from the WSR-88D analysis is 6.3 km. The difference in advection speeds between the rolls and cells allows the separation between the two in frequency even though they are of similar spatial size.

The roll-scale wavelet amplitude (averaged over the period range 39.3–55.6 min) is shown on the right-hand axis in Fig. 5a. Overall, there is reasonably good agreement between the linearity as estimated by the cloud radar (roll-scale wavelet amplitude) and that estimated by the WSR-88D (HAR); the correlation coefficient is 0.34, which is statistically significant at the <1% error level (Young 1962). Although we have excluded points after 0140 UTC for which the WSR-88D reflectivity is clearly too low to provide accurate HAR (as discussed in section 3), the increase in scatter in the HAR values between 1900 and 0140 UTC likely indicates developing problems with the HAR analysis. Fortunately, determination of linear organization from the cloud radar (via wavelet analysis of vertical velocity) needs only reflectivity above the noise level of the radar within the approximately 3 m × 50 m footprint. Based on the good relationship between the HAR and roll-scale wavelet amplitude between 1217 and 1900 UTC, and its lack of dependency on reflectivity, we will use the roll-scale wavelet amplitude as the indicator of linear organization.

(iv) Large scale (157.2–222.4 min): A possible physical explanation for the large-scale variability is mesoscale gravity wave activity, although we have no evidence to support such a claim. Because the length of the time series is only about 5.7 times the large-scale period, conclusions about the time variability of this scale are not possible. The corresponding spatial scale is unknown.

In Fig. 6b, the global (i.e., time-averaged throughout the analysis period) vertical velocity spectrum is plotted in area-preserving form, which highlights the relative contribution of each scale to the total variance. The peaks correspond to the four period bands: turbulence, cells, rolls, and large scales. There is a factor of 4 difference between the peak periods associated with the cell and roll scales, and with the roll and large scales. Analysis of shorter time segments of the data revealed slightly different peaks that are not integer multiples of one another; thus, this is not an artifact of the analysis technique.

The wavelet analysis was performed for time series of vertical velocity at several levels between 630 m AGL (near the average cloud base) and 900 m AGL (near the average cloud top). For all heights within cloud, the turbulence-scale peak is the largest contributor to the total variance. The cell-scale peak is of similar magnitude, but is narrower than the turbulence-scale peak. The roll-scale peak is also present at all in-cloud heights, but its contribution to the total variance is comparatively low. The large-scale peak contributes very little to the total variance. The frequency structure changes little with height, as is expected above the surface layer (e.g., Kaimal et al. 1976; Young 1987; Khanna and Brasseur 1998).

Contributions to the vertical velocity due to different physical structures are separated by high-pass filtering the data for the turbulence scale and bandpass filtering for the cell, roll, and large scales. Both the high-pass and bandpass filters employed are based on fast Fourier transforms (FFTs). The resulting vertical velocities separated into the four scales are shown in Fig. 7, for the data at 720 m (0.81 z_i). The cutoff periods used are those suggested by the wavelet analysis (Fig. 6b): turbulence-scale vertical velocity, w^t (<8.3 min); cell-scale vertical velocity, w^c (8.3–16.5 min); roll-scale vertical velocity, w^r (39.3–55.6 min); and large-scale vertical velocity, w^l (157.2–222.4 min). The three cycles in the roll-scale wavelet amplitude are also apparent in the changing amplitude of the roll-scale vertical velocity (both shown in Fig. 7). Both increasing and decreasing the width of the bandpass filters by 50% produced similar results when scaled by the total variance within each

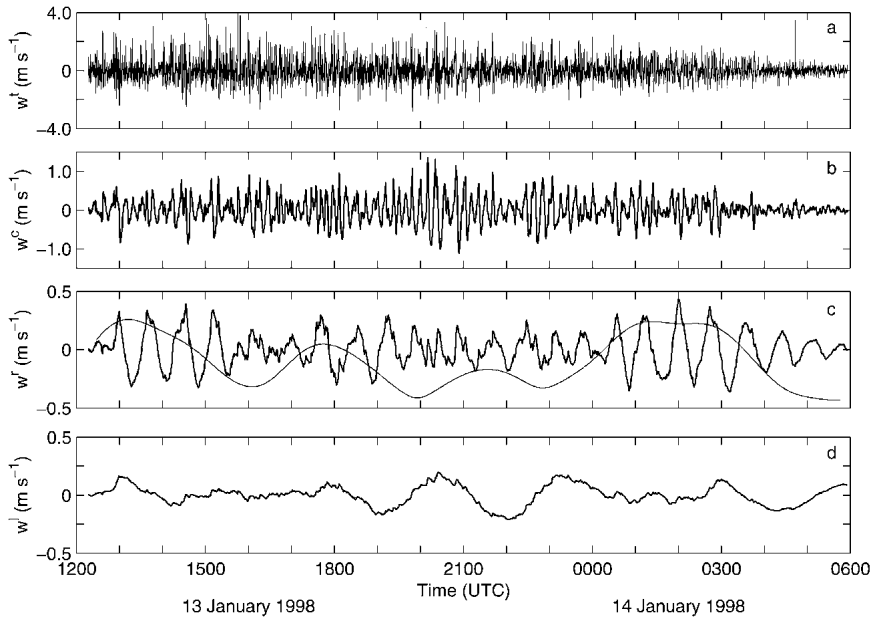

FIG. 7. Filtered vertical velocity at a height of 720 m (midcloud) for the (a) turbulence scale (<8.3 min), (b) cell scale (8.3–16.5 min), (c) roll scale (39.3–55.6 min), and (d) large scale (157.2–222.4 min). Corresponding spatial sizes are 100 m–3.7 km for the turbulence scale and 3.7–7.4 km for the cell scale. The average wavelength of the rolls is 6.3 km. The roll-scale wavelet amplitude (thin line) is overlaid on the roll-scale vertical velocity trace for comparison. Note the different scales on the *y* axes.

band. The reliability of the large-scale results is questionable, and they are excluded from further discussion.

5. Discussion

The most straightforward explanation for the mode switches is changes in atmospheric conditions such as surface fluxes, shear, or their ratio. We now consider these possible causes, while leaving discussion of alternate mechanisms to Part II. Horizontal roll vortices and associated cloud streets are most often found in neutral to slightly unstable boundary layers in both modeling (e.g., Deardorff 1972; Sykes and Henn 1989; Khanna and Brasseur 1998; Glendening 2000) and observational studies (e.g., LeMone 1973; Grossman 1982; Weckwerth et al. 1997). Other studies, however, have indicated that rolls can also occur in very unstable conditions. For example, Kelly (1984) and Kristovich (1993) documented horizontal roll convection in the boundary layer over Lake Michigan during unstable, lake-effect conditions. Christian and Wakimoto (1989), in their triple-Doppler radar analysis, found evidence for rolls over northeastern Colorado during conditions predicted by many past studies to favor nonroll convection. Lidar observations by Ferrare et al. (1991) also revealed roll circulations in very unstable conditions. Some authors have found parameters such as low-level shear (e.g., Kristovich 1993) to be the determining factor for linear organization. We investigate changes in shear and stability over the course of the 18 h of observations to establish whether there is any relationship with the observed mode changes.

a. Vertical shear of the horizontal wind

Many authors have found vertical shear of the horizontal wind (hereafter, shear) to be important to roll formation. For example, Kuettner (1971) suggested high wind shear curvature as a criterion for rolls, while Miura (1986) found boundary layer wind shear to be the determining factor. Kristovich (1993), Kristovich et al. (1999), and Cooper et al. (2000) argued that along-roll shear at low levels is critical for roll formation in lake-effect conditions, and a similar conclusion was made by Weckwerth et al. (1997) for rolls in east-central Florida.

The boundary layer mean wind shear, calculated between each set of two vertically adjacent heights and averaged throughout the boundary layer, for the upwind (95–375 m) and downwind ISS profiler data (53–837 m) is shown in Figs. 8a and 8b, respectively. The downwind time-averaged boundary layer mean shear is about half the magnitude of the upwind equivalent, reflecting the effect of the strong mixing caused by the addition of heat and moisture from the lake. The downwind shore ISS site is sheltered by sand dunes, undoubtedly affecting the vertical profiles, especially in the surface layer and lower part of the boundary layer. The trends, however, should be at least grossly repre-

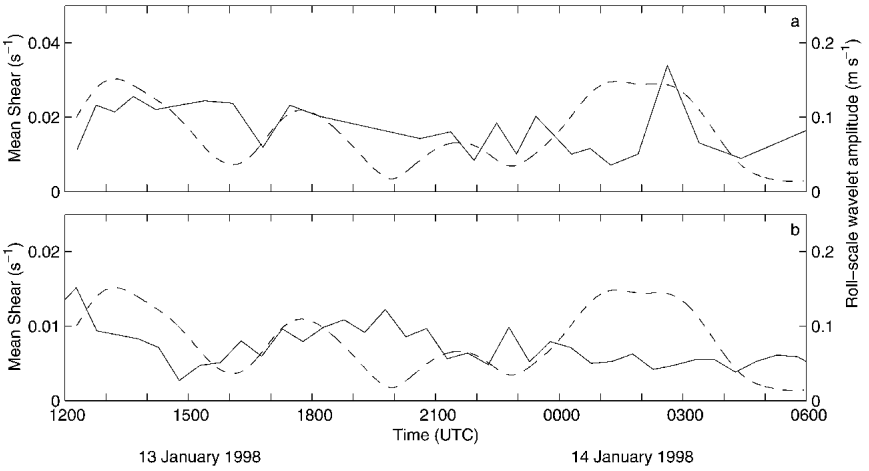

FIG. 8. The boundary layer mean wind shear, calculated between each set of two vertically adjacent heights and averaged throughout the boundary layer, for (a) upwind and (b) downwind ISS profiler data. The roll-scale wavelet amplitude is represented by dashed lines. The times indicated in (a) for the mean shear are the estimated times that the parcels from the upwind shore reached the downwind shore. Note the difference in scale between (a) and (b) for the mean shear.

sented. Since the random error associated with the profiler wind speeds used to calculate the boundary layer mean wind shear is on the order of 0.5 m s^{-1} under ideal conditions (Cohn and Goodrich 2002), the boundary layer mean wind shear is known only to within ± 0.03 s^{-1}, which is large compared to the variability observed. The time-averaged (throughout the analysis period) boundary layer mean shear for the downwind ISS site (9×10^{-3} s^{-1}) is above the critical level (10^{-3} s^{-1}) for roll formation found by Miura (1986). In fact, the boundary layer mean shear never goes below the critical level during the analysis period. The correlation coefficients of the upwind and downwind boundary layer mean shear with the roll-scale wavelet amplitude are not statistically significant. Within the limits of the available measurements, the organization does not appear to be controlled by the boundary layer mean shear.

Using the time-averaged roll orientation from the autocorrelation analysis of the WSR-88D data, the low-level shear (calculated between the surface measurement and the lowest profiler measurement) is separated into cross-roll and along-roll shear (Figs. 9a and 9b) for the upwind and downwind sites, respectively. The correlation coefficients of the low-level shears are not statistically significant for the upwind or downwind sites.

The criterion for rolls suggested by Kuettner (1971) is boundary layer wind shear curvature greater than 10^{-5} m^{-1} s^{-1}. The boundary layer mean wind shear curvature, estimated as the boundary layer mean wind speed (Fig. 3h) divided by the boundary layer depth (Fig. 2) squared (Kristovich 1993), has a trend similar to the boundary layer wind speed, generally decreasing while the roll organization waxes and wanes. The boundary layer wind shear curvature thus does not appear to play a role in the mode switching observed in this case.

When the ocean water temperature was more than 4°C higher than the air temperature, Woodcock (1942) reported wind speed to be a predictor of linear or circular soaring by herring gulls. For wind speeds less than 7 m s^{-1} (presumably measured near the surface), Woodcock (1942) observed mostly circular soaring and presumed the convection to be cellular. For wind speeds greater than 7 m s^{-1}, Woodcock (1942) observed mostly linear soaring associated with rolls. Weckwerth et al. (1997) also reported a minimum wind speed necessary for rolls: 5.5 m s^{-1} for the mean boundary layer wind speed or 3.0 m s^{-1} for the surface wind speed. The surface wind speed for the Montague ISS site generally decreased with time throughout the analysis period (Fig. 3h). During this time three cycles of linear organization followed by cellular organization occurred. Thus in this case, changes in wind speed did not appear to incite the changes in convective organization.

b. Buoyancy

Weckwerth et al. (1999) suggested that the formation of rolls is dependent upon the magnitude of the buoyancy flux. The surface sensible (H) and latent (E) heat fluxes across the lake surface–air interface are defined as (e.g., Chou 1993)

$$H \equiv \rho c_p \overline{w\theta}|_s \tag{1a}$$

and

$$E \equiv \rho L_v \overline{wq}|_s, \tag{1b}$$

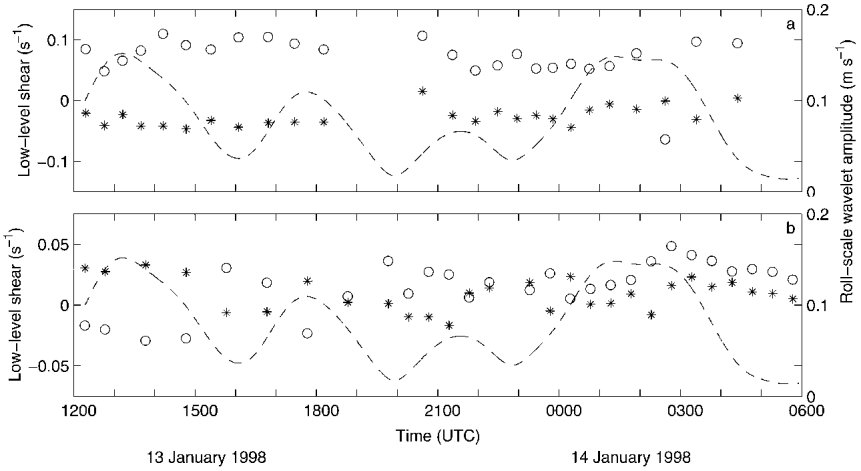

FIG. 9. Low-level shear calculated between the lowest profiler measurement (95 m for the upwind site and 53 m for the downwind site) and the surface station measurement (10 m) for the (a) upwind and (b) downwind ISS sites. Open circles are along-roll shear and stars are cross-roll shear. On the right-hand axis is the roll-scale wavelet amplitude. The times indicated in (a) for the low-level shear are the estimated times that the parcels from the upwind shore reached the downwind shore.

where ρ is the air density, w is the deviation from the mean vertical velocity, θ is the deviation from the mean potential temperature, q is the deviation from the mean specific humidity, c_p is the heat capacity at constant pressure for air, and L_v is the latent heat of vaporization for water at 0°C. The subscript s indicates that the fluxes are surface values. For this study, the surface heat fluxes are parameterized according to the bulk transfer formulas as (Chou and Atlas 1982; Chou 1993; Kristovich et al. 1999)

$$H_{\text{bulk}} = \rho c_p C_H (U - U_s)(T_s - T) \tag{2a}$$

and

$$E_{\text{bulk}} = \rho L_v C_E (U - U_s)(\rho_{v,s} - \rho_v), \tag{2b}$$

where ρ_v is the water vapor density, U is the wind speed at 10 m, and T is the temperature at 2 m. The heat capacity c_p is assumed to be a constant value of 1004.5 J kg^{-1} K^{-1}, and the nondimensional bulk transfer coefficients for heat and moisture, C_H and C_E, are both assumed equal to 1.5×10^{-3} (Arya 1988). The water vapor density $\rho_{v,s}$ is taken to be the saturation value for T_s, the lake surface temperature (+4°C). The wind speed at the surface U_s is assumed to be zero. The surface latent and sensible heat fluxes are calculated using the surface data from the Sheboygan (Fig. 10a) and Montague (Fig. 10c) ISS sites. As noted by Kristovich et al. (1999), the trends in the fluxes obtained by the bulk transfer method should be the same as those derived from the eddy correlation technique, although the magnitudes may differ.

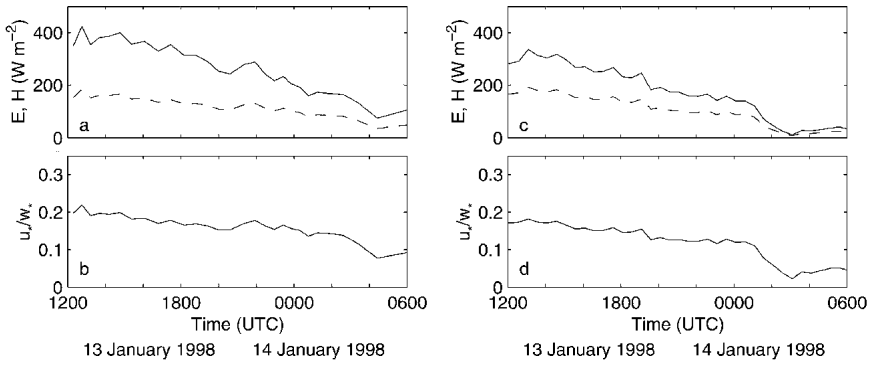

FIG. 10. (a), (c) Sensible heat flux (solid line) and latent heat flux (dashed line) for upwind (Sheboygan) and downwind (Montague) sites, respectively. (b), (d) The ratio of the friction velocity to the convective velocity scale, u_*/w_*, for upwind and downwind sites, respectively. The times indicated in (a) and (b) are the estimated times that the parcels from the upwind shore reached the downwind shore.

On the upwind shore of the lake, the surface sensible (latent) heat flux peaked at about 385 W m^{-2} (180 W m^{-2}) before the beginning of the analysis period (1217 UTC), then decreased monotonically to less than 100 W m^{-2} (40 W m^{-2}). The downwind surface sensible (latent) heat flux monotonically decreased from near 350 W m^{-2} (180 W m^{-2}) at the beginning of the analysis period (1217 UTC) to 120 W m^{-2} (80 W m^{-2}) at 0140 UTC, then dropped to less than 50 W m^{-2} (25 W m^{-2}) after the land breeze developed. This monotonic decrease in the surface fluxes occurs during the period when the mesoscale organization fluctuates between linear and cellular organization, suggesting that the surface fluxes played no direct role in the mode switching.

c. Stability parameter

Several authors have found limiting values of the nondimensional ratios u_*/w_* or $-z_i/L$ as criteria for boundary layer roll development. The quantities u_*/w_* (where u_* is the friction velocity and w_* is the convective velocity scale) and $-z_i/L$ (where L is the Monin–Obukhov length) are estimates of the relative amount of wind shear compared to thermal instability.

Assuming the surface wind speed is zero, the friction velocity u_* may be estimated as

$$u_* = \sqrt{C_D U^2}, \tag{3}$$

where C_D is the constant drag coefficient, taken to be 1.5×10^{-3} (Arya 1988). One way of calculating the convective velocity scale w_* is

$$w_* = \left[\frac{g z_i H(1 + 0.07/B)}{\rho T c_p}\right]^{1/3}, \tag{4}$$

where the $0.07/B$ term is used to account for the latent heat flux (Arya 1988), and B is the Bowen ratio. For the Bowen ratios observed in this case, the correction to the total heat flux by the latent heat flux term is 3%–5%.

The Monin–Obukhov length L may be estimated as (e.g., Grossman 1982)

$$L = \frac{-\rho c_p T u_*^3}{kgH(1 + 0.07/B)}, \tag{5}$$

where k is the von Kármán constant (taken to be 0.4). In convective conditions, the Monin–Obukhov length is the lowest height above the earth's surface at which buoyant production of turbulent kinetic energy is greater than that of shear production. The quantity $-z_i/L$ written in terms of u_*/w_* is $-z_i/L = k[u_*/w_*]^{-3}$.

The quantity u_*/w_* was similar in magnitude upwind and downwind of the lake. As shown in Fig. 10b, the upwind u_*/w_* monotonically decreased from about 0.18 to 0.05, corresponding to $-z_i/L = 69$–3200. On the downwind shore, the ratio u_*/w_* decreased roughly linearly from 0.18 at 1217 UTC to about 0.12 at 0140 UTC, as shown in Fig. 10d. The corresponding values for $-z_i/L$ are 69 to 231. At 0140 UTC, u_*/w_* at the downwind shore dropped to 0.04 as a result of a dramatic drop in wind speed associated with a land breeze.

These values for u_*/w_* are much less than the criterion for linearly organized convection of 0.35 predicted by the numerical experiments of Sykes and Henn (1989) and are in the regime in which Grossman (1982) found only random cells during the Barbados Oceanographic and Meteorological Experiment ($-z_i/L > 21.4$; $u_*/w_* < 0.27$). Even if the wind speed at the downwind ISS site is doubled (as perhaps suggested from comparison of the Muskegon and Montague data), the average u_*/w_* at the downwind shore (Fig. 10d) only increases from 0.13 to 0.20, which is still less than the generally quoted critical value of 0.35 (Sykes and Henn 1989). There have, however, been other observations of rolls in atmospheric conditions in which rolls are not expected. Kelly (1984), Christian and Wakimoto (1989), Ferrare et al. (1991), and Kristovich (1993) documented rolls in the same range of shear to thermal instability found in the present study.

While the convective organization switches modes on several occasions during the analysis period, both the upwind (Fig. 10b) and downwind (Fig. 10d) u_*/w_* decrease throughout the analysis period. The balance between shear and thermal instability, as measured by u_*/w_* (or $-z_i/L$), is therefore not a likely cause of the convective mode switching in this case. At both the upwind and downwind ISS sites, the value of u_*/w_* is less than 0.2, or equivalently, the value of $-z_i/L$ is greater than 50.

6. Conclusions

Vertically pointing cloud radar and two-dimensional WSR-88D data both reveal transient linear organization during a lake-effect event. Wavelet analysis of vertical velocity from a cloud radar indicates three distinct scales of motion: turbulence scale, cell scale, and roll scale (and possibly a fourth, which is not discussed.) Cycles in the roll-scale wavelet amplitude give evidence for the organization switching between linear and cellular. These cycles are also apparent in the horizontal aspect ratio (HAR) of the two-dimensional autocorrelation of the WSR-88D reflectivity images. The period expected from vertically pointing cloud radar based on the WSR-88D images agrees to within 10% of the actual value determined by wavelet analysis, and the correlation between the roll-scale wavelet amplitude and the HAR is statistically significant.

The duration of measurements is critical to the observation of the mode switching; in this case, the duration of the radar measurements is nearly 18 h, encompassing three cycles of marginally linearly organized convection switching to unorganized cellular convection and back again. While there are a few observations of mode switching (Braham 1986; Kristovich et al. 1999;

Weckwerth et al. 1999), a likely cause for the scarcity of observations is the duration of continuous measurements required. This study highlights the danger of observing rolls and the associated conditions for a short time compared to the mode-switching frequency and making conclusions about the conditions necessary to form rolls. This result may explain, in part, the discrepancy between the ranges of atmospheric conditions in which rolls are observed—the datasets may not have been long enough to capture the essential physics, especially for marginal cases.

There are discrepancies in the literature as to the atmospheric conditions required for roll formation. The present lake-effect event, with large positive buoyancy flux and only moderate shear, is not within the range of buoyancy parameters most often associated with rolls. Within the limits of the available observations, neither boundary layer mean shear nor low-level shear was correlated with the observed transient linear organization. The stability parameter u_*/w_* decreased monotonically from 0.2 to less than 0.1 while the organization cycled between linear and cellular. Changes in the surface buoyancy flux are also not correlated to the changes in organization, suggesting that there may be a different factor affecting the organization. In Part II we investigate scale interactions as a possible contributor to the observed mode switching.

Acknowledgments. We would like to acknowledge George Young, John Wyngaard, Jerry Harrington, Eugene Clothiaux, David Babb, Charles Pavloski, Laura Hinkelman, and Dave Kristovich for many helpful discussions. The ISS data were obtained from E. Miller (NCAR/ATD). Lake surface temperatures were provided by the Great Lakes Environmental Research Laboratory (GLERL) Coastwatch program. The PSU radar was hosted in Muskegon by the GLERL Lake Michigan Field Station. Wavelet analysis software was provided by C. Torrence and G. Compo and is available online at http://paos.colorado.edu/research/wavelets/. This work was supported by the National Science Foundation under Grants ATM-9596107, ATM-9629343, ATM-9873643, and ATM-0127360. N. Miles was also supported by a Pennsylvania State University Graduate School Dissertation Fellowship.

REFERENCES

Agee, E. M., and S. R. Gilbert, 1989: An aircraft investigation of mesoscale convection over Lake Michigan during the 10 January 1984 cold air outbreak. *J. Atmos. Sci.,* **46,** 1877–1897.

Arya, S. P., 1988: *Introduction to Micrometeorology.* Academic Press, 307 pp.

Atkinson, B. W., and J. W. Zhang, 1996: Mesoscale shallow convection in the atmosphere. *Rev. Geophys.,* **34,** 403–431.

Babb, D. M., J. Verlinde, and B. W. Rust, 2000: The removal of turbulent broadening in radar Doppler spectra using linear inversion with double-sided constraints. *J. Atmos. Oceanic Technol.,* **17,** 1583–1595.

Braham, R. R., Jr., 1983: The Midwest snow storm of 8–11 December 1977. *Mon. Wea. Rev.,* **111,** 253–272.

——, 1986: Cloud and motion fields in open cell convection over Lake Michigan. Preprints, *23rd Conf. on Radar Meteorology and Conf. on Cloud Physics,* Snowmass, CO, Amer. Meteor. Soc., JP202–JP205.

——, and D. A. R. Kristovich, 1996: On calculating the buoyancy of cores in a convective boundary layer. *J. Atmos. Sci.,* **53,** 654–658.

Brooks, I. M., and D. P. Rogers, 1997: Aircraft observations of boundary layer rolls off the coast of California. *J. Atmos. Sci.,* **54,** 1834–1849.

Burrows, W. R., 1991: Objective guidance for 0–24-hour and 24–48-hour mesoscale forecasts of lake-effect snow using CART. *Wea. Forecasting,* **6,** 357–378.

Chang, S. S., and R. R. Braham Jr., 1991: Observational study of a convective internal boundary layer over Lake Michigan. *J. Atmos. Sci.,* **48,** 2265–2279.

Chou, S.-H., 1993: A comparison of airborne eddy correlation and bulk aerodynamic methods for ocean–air turbulent fluxes during cold-air outbreaks. *Bound.-Layer Meteor.,* **64,** 75–100.

——, and D. Atlas, 1982: Satellite estimates of ocean–air heat fluxes during cold air outbreaks. *Mon. Wea. Rev.,* **110,** 1434–1450.

Christian, T. W., and R. M. Wakimoto, 1989: The relationship between radar reflectivities and clouds associated with horizontal roll convection on 8 August 1982. *Mon. Wea. Rev.,* **117,** 1530–1544.

Chui, C. K., 1992: *An Introduction to Wavelets.* Academic Press, 264 pp.

Clothiaux, E. E., M. A. Miller, B. A. Albrecht, T. P. Ackerman, J. Verlinde, D. M. Babb, R. M. Peters, and W. J. Syrett, 1995: An evaluation of a 94-GHz radar for remote sensing of cloud properties. *J. Atmos. Oceanic Technol.,* **12,** 201–229.

Cohn, S. A., and R. K. Goodrich, 2002: Radar wind profiler radial velocity: A comparison with Doppler lidar. *J. Appl. Meteor.,* **41,** 1277–1282.

Cooper, K. A., M. R. Hjelmfelt, R. G. Derickson, D. A. R. Kristovich, and N. F. Laird, 2000: Numerical simulation of transitions in boundary layer convective structures in a lake-effect snow event. *Mon. Wea. Rev.,* **128,** 3283–3295.

Cressman, G. P., 1959: An operational objective analysis scheme. *Mon. Wea. Rev.,* **87,** 367–374.

Deardorff, J. W., 1972: Numerical investigation of neutral and unstable planetary boundary layers. *J. Atmos. Sci.,* **29,** 91–115.

Etling, D., and R. A. Brown, 1993: Roll vortices in the planetary boundary layer: A review. *Bound.-Layer Meteor.,* **65,** 215–248.

Ferrare, R. A., J. L. Schols, E. W. Eloranta, and R. Coulter, 1991: Lidar observations of banded convection during BLX83. *J. Appl. Meteor.,* **30,** 312–326.

Gabor, D., 1946: Theory of communications. *J. Inst. Electron. Eng.,* **93,** 429–457.

Giangrande, S. E., D. M. Babb, and J. Verlinde, 2001: Processing millimeter wave profiler radar spectra. *J. Atmos. Oceanic Technol.,* **18,** 1577–1583.

Glendening, J. W., 2000: Budgets of lineal and nonlineal turbulent kinetic energy under strong shear conditions. *J. Atmos. Sci.,* **57,** 2297–2318.

Grossman, R. L., 1982: An analysis of vertical velocity spectra obtained in the BOMEX fair-weather, trade-wind boundary layer. *Bound.-Layer Meteor.,* **23,** 323–337.

Holroyd, E. W., III, 1971: Lake-effect cloud bands as seen from weather satellites. *J. Atmos. Sci.,* **28,** 1165–1170.

Kaimal, J. C., J. C. Wyngaard, D. A. Haugen, O. R. Coté, Y. Izumi, S. J. Caughey, and C. J. Readings, 1976: Turbulence structure in the convective boundary layer. *J. Atmos. Sci.,* **33,** 2152–2169.

Kelly, R. D., 1984: Horizontal roll and boundary-layer interrela-

tionships observed over Lake Michigan. *J. Atmos. Sci.,* **41,** 1816–1826.
Khanna, S., and J. G. Brasseur, 1998: Three-dimensional buoyancy- and shear-induced local structure of the atmospheric boundary layer. *J. Atmos. Sci.,* **55,** 710–743.
Kiemle, C., G. Ehret, and K. J. Davis, 1998: Airborne lidar studies of the entrainment zone. *Proc. 19th Int. Laser-Radar Conf.,* Annapolis, MD, NASA, NASA/CP-1998-207671/PT1, 395–398.
Kristovich, D. A. R., 1993: Mean circulations of boundary-layer rolls in lake-effect snow storms. *Bound.-Layer Meteor.,* **63,** 293–315.
——, N. F. Laird, M. R. Hjelmfelt, R. G. Derickson, and K. A. Cooper, 1999: Transitions in boundary layer meso-γ convective structures: An observational case study. *Mon. Wea. Rev.,* **127,** 2895–2909.
——, and Coauthors, 2000: The Lake-Induced Convection Experiment and the Snowband Dynamics Project. *Bull. Amer. Meteor. Soc.,* **81,** 519–542.
——, N. F. Laird, and M. R. Hjelmfelt, 2003: Convective evolution across Lake Michigan during a widespread lake-effect snow event. *Mon. Wea. Rev.,* **131,** 643–655.
Kuettner, J., 1959: The band structure of the atmosphere. *Tellus,* **11,** 267–294.
——, 1971: Cloud bands in the earth's atmosphere. *Tellus,* **23,** 404–425.
Lau, K.-M., and H. Weng, 1995: Climate signal detection using wavelet transform: How to make a time series sing. *Bull. Amer. Meteor. Soc.,* **76,** 2391–2402.
LeMone, M. A., 1973: The structure and dynamics of horizontal roll vortices in the planetary boundary layer. *J. Atmos. Sci.,* **30,** 1077–1091.
Lohou, F., A. Druilhet, and B. Campistron, 1998: Spatial and temporal characteristics of horizontal rolls and cells in the atmospheric boundary layer based on radar and in situ observations. *Bound.-Layer Meteor.,* **89,** 407–444.
Miles, N. L., 2002: Observations of transient linear organization and nonlinear scale interactions in lake-effect clouds. Ph.D. dissertation, The Pennsylvania State University, 103 pp.
——, and J. Verlinde, 2005: Observations of transient linear organization and nonlinear scale interactions in lake-effect clouds. Part II: Nonlinear scale interactions. *Mon. Wea. Rev.,* **133,** 692–706.
Miura, Y., 1986: Aspect ratios of longitudinal rolls and convection cells observed during cold air outbreaks. *J. Atmos. Sci.,* **43,** 26–39.
Niziol, T. A., 1987: Operational forecasting of lake effect snowfall in western and central New York. *Wea. Forecasting,* **2,** 310–321.
Oye, R., and M. Case, 1994: REORDER: A program for gridding radar data: Installation and use manual for the UNIX version. Field Observing Facility, National Center for Atmospheric Research, 29 pp. [Available from Atmospheric Technology Division, NCAR, P.O. Box 3000, Boulder, CO 80307.]
Renfrew, I. A., and G. W. K. Moore, 1999: An extreme cold-air outbreak over the Labrador Sea: Roll vortices and air–sea interaction. *Mon. Wea. Rev.,* **127,** 2379–2394.
Sykes, R. I., and D. S. Henn, 1989: Large-eddy simulation of turbulent sheared convection. *J. Atmos. Sci.,* **46,** 1106–1118.
Torrence, C., and G. P. Compo, 1998: A practical guide to wavelet analysis. *Bull. Amer. Meteor. Soc.,* **79,** 61–78.
Walter, B. A., 1980: Wintertime observations of roll clouds over the Bering Sea. *Mon. Wea. Rev.,* **108,** 2024–2031.
Weckwerth, T. M., J. W. Wilson, R. M. Wakimoto, and N. A. Crook, 1997: Horizontal convective rolls: Determining the environmental conditions supporting their existence and characteristics. *Mon. Wea. Rev.,* **125,** 505–526.
——, T. W. Horst, and J. W. Wilson, 1999: An observational study of the evolution of horizontal convective rolls. *Mon. Wea. Rev.,* **127,** 2160–2179.
Woodcock, A. H., 1942: Soaring over the open sea. *Sci. Mon.,* **55,** 226–232.
Young, G. S., 1987: Mixed layer spectra from aircraft measurements. *J. Atmos. Sci.,* **44,** 1251–1256.
——, B. K. Cameron, and E. E. Hebble, 2000: Observations of the entrainment zone in a rapidly entraining boundary layer. *J. Atmos. Sci.,* **57,** 3145–3160.
——, D. A. R. Kristovich, M. R. Hjelmfelt, and R. C. Foster, 2002: Supplement to rolls, streets, waves, and more. *Bull. Amer. Meteor. Soc.,* **83,** 1001.
Young, H. D., 1962: *Statistical Treatment of Experimental Data.* McGraw-Hill, 172 pp.